Radiative and Dynamic Controls on Atmospheric Heat Transport over Different Planetary Rotation Rates®

Tyler Cox^a, Kyle C. Armour, ^b Gerard H. Roe, ^c Aaron Donohoe, ^d and Dargan M. W. Frierson^a

^a Department of Atmospheric Sciences, University of Washington, Seattle, Washington
^b School of Oceanography and Department of Atmospheric Sciences, University of Washington, Seattle, Washington
^c Department of Earth and Space Sciences, University of Washington, Seattle, Washington
^d Polar Science Center and Applied Physics Laboratory, University of Washington, Seattle, Washington

(Manuscript received 10 July 2020, in final form 21 January 2021)

ABSTRACT: Atmospheric heat transport is an important piece of our climate system, yet we lack a complete theory for its magnitude or changes. Atmospheric dynamics and radiation play different roles in controlling the total atmospheric heat transport (AHT) and its partitioning into components associated with eddies and mean meridional circulations. This work focuses on two specific controls: a radiative one, namely atmospheric radiative temperature tendencies, and a dynamic one, the planetary rotation rate. We use an idealized gray radiation model to employ a novel framework to lock the radiative temperature tendency and total AHT to climatological values, even while the rotation rate is varied. This setup allows for a systematic study of the effects of radiative tendency and rotation rate on AHT. We find that rotation rate controls the latitudinal extent of the Hadley cell and the heat transport efficiency of eddies. Both the rotation rate and radiative tendency influence the strength of the Hadley cell and the strength of equator—pole energy differences that are important for AHT by eddies. These two controls do not always operate independently and can reinforce or dampen each other. In addition, we examine how individual AHT components, which vary with latitude, sum to a total AHT that varies smoothly with latitude. At slow rotation rates the mean meridional circulation is most important in ensuring total AHT varies smoothly with latitude, while eddies are most important at rotation rates similar to, and faster than, those of Earth.

KEYWORDS: Eddies; Energy transport; Hadley circulation; Mass fluxes/transport; Meridional overturning circulation; Radiation budgets

1. Introduction

Atmospheric heat transport (AHT) is an integral part of our climate system. AHT is responsible for the habitable conditions at most latitudes, exporting energy from the warm tropics to the cold polar regions (e.g., Pierrehumbert 2010), and is also closely tied to the spatial patterns of temperature and hydrology (e.g., Held and Soden 2006; Siler et al. 2018). Despite the existence of several conceptual perspectives of AHT and its importance for local climate, there is currently no accepted complete theory for the climatological magnitude of AHT, or its predicted changes under climate change (e.g., Armour et al. 2019). An improved understanding of the basic controls on AHT is needed.

Throughout this work AHT is referring to the mass-weighted, vertically and zonally integrated meridional flux of moist static energy. AHT can be partitioned into three components (e.g., Holton and Hakim 2013): 1) mean meridional overturning circulations (MMC), comprising the Hadley, Ferrel, and polar cells; 2) stationary eddies, such as semi-permanent undulations of the jet stream; and 3) transient eddies, such as midlatitude storms. While each of these three AHT components have their own complex

© Supplemental information related to this paper is available at the Journals Online website: https://doi.org/10.1175/JCLI-D-20-0533.s1.

Corresponding author: Tyler Cox, tylersc@uw.edu

latitudinal structure, they must behave in a way that satisfies both dynamic and radiative controls at every latitude. AHT varies smoothly with latitude in coordination with the smoothly varying top-of-atmosphere radiation budget (Trenberth and Stepaniak 2003). The radiative control does not alone cause smoothly varying AHT as AHT itself influences the radiation. Radiation can also influence individual AHT components such as the Hadley cell (Merlis 2015).

There are also strong dynamical constraints on AHT and its partitioning coming from factors such as the location of mountain ranges (e.g., Brayshaw et al. 2009; Saulière et al. 2012; White et al. 2017) or the planetary rotation rate (e.g., Hunt 1979; Del Genio and Suozzo 1987; Walker and Schneider 2006; Vallis and Farneti 2009; Kaspi and Schneider 2013; Kaspi and Showman 2015; Liu et al. 2017). For instance, altering the rotation rate Ω results in large changes to both total AHT and its components, including the Hadley cell expanding poleward and dominating AHT at slower rotation rates (e.g., Walker and Schneider 2006; Vallis and Farneti 2009; Guendelman and Kaspi 2019). Previous work has found that the rotation rate is one of the strongest controls over Hadley cell extent (e.g., Del Genio and Suozzo 1987; Navarra and Boccaletti 2002; Kaspi and Showman 2015; Guendelman and Kaspi 2019; Hill et al. 2019; Singh 2019). At faster rotation rates, a decrease in eddy length scale results in less efficient AHT by eddies (Kaspi and Showman 2015; Liu et al. 2017). The Hadley cell also diminishes in strength at faster rotation rates (e.g., Del Genio and Suozzo 1987; Navarra and Boccaletti 2002; Kaspi and Showman 2015; Wang et al. 2018).

The ways in which AHT components adjust to satisfy the radiative and dynamic controls in our current climate, as well as in past and future climates, is still an area of active research (Armour et al. 2019; Donohoe et al. 2020). One hypothesis is that transient eddies are a flexible AHT component, capable of responding to radiative and dynamical controls to ensure that both are satisfied simultaneously (Trenberth and Stepaniak 2003; Armour et al. 2019; Donohoe et al. 2020). This idea is based on the ability of transient eddies to smooth atmospheric heating anomalies, which results in smoothly varying AHT (Farneti and Vallis 2013; Donohoe et al. 2020). Previous studies have shown that transient eddies are less important for AHT in the time mean at slow rotation rates (e.g., Del Genio and Suozzo 1987; Kaspi and Showman 2015) but have not explored if transient eddies are the most flexible AHT component at these slow rotation rates. In this study we test the transienteddy compensation hypothesis to determine its limitations in climates where transient eddies play little role, and explore AHT and its partitioning over a range of planetary rotation rates.

We also aim to assess the relative roles of dynamic and radiative controls on AHT. To do so, we employ a novel modeling framework wherein we can hold total AHT fixed by prescribing the climatological atmospheric radiation budget, even while altering the planetary rotation rate. Comparing simulations with fixed AHT, but altered rotation rates, allows us to explore how atmospheric circulations respond to a change in a fundamental constraint on their dynamics, changes in planetary rotation rate, while their radiative control remains constant, producing the same total AHT. Comparing simulations at a given rotation rate with AHT that is either fixed or free to evolve as normal allows us to explore how atmospheric circulations respond to changes in radiation. This framework thus offers the ability to disentangle the relative roles of dynamics and radiation on atmospheric circulations and AHT, and to study their interactions in a way that is not possible in observations or comprehensive general circulation models.

This article is organized as follows. In section 2 we introduce the modeling framework and describe how we constrain the radiative energy budget. In section 3a we discuss how our model alterations that constrain the radiative energy budget affect the control climate. We then explore how changes in the planetary rotation rate and atmospheric radiation affect AHT by analyzing the role of the MMC (section 3c) and eddies (section 3d) separately. In section 4 we discuss the individual roles of, and interactions between, the planetary rotation rate and radiative energy budget in controlling AHT and its partitioning.

2. Methods

Model overview

We use an aquaplanet, gray radiation model (GRaM) with all parameters set to the original values from Frierson et al. (2006), except we use a simplified Betts-Miller convection scheme as in Frierson (2007) and alter some of the radiative code as described in the following paragraphs. As in Frierson et al. (2006), this model absorbs shortwave radiation at the surface, but not in the atmosphere, and has a spatially uniform albedo of 0.31. Longwave radiation is absorbed and emitted at the surface and in the atmosphere via a prescribed broadband

optical depth that varies with latitude and height to mimic the optical properties of water vapor. There is no seasonal or diurnal cycle, no continents, and no topography. As a result, stationary eddies are negligible, leaving transient eddies and the mean meridional circulations to provide all AHT. Hereafter, all references to eddies refer to transient eddies. The model uses a spectral dynamical core with resolution of T42, which corresponds to roughly 2.8° horizontal resolution, and has 25 vertical levels. All results presented here are at T42 resolution. We also ran the model at a higher T85 resolution, but found no significant changes to the conclusions of this study. The atmosphere is coupled to a slab ocean with uniform 2.4-m depth. There is no ocean heat transport (no prescribed "Q-fluxes" in the slab ocean), and therefore zero surface energy flux at equilibrium.

We perform two sets of numerical experiments. In the first set, we perform six simulations with varying planetary rotation rates of 1/16, 1/8, 1/4, 1/2, 1, and 2 times Earth's normal rotation rate of $\Omega = 7.292 \times 10^{-5} \, \text{rad s}^{-1}$. These are referred to here as $1/16\times$, $1/8\times$, $1/4\times$, $1/2\times$, $1\times$, and $2\times$, respectively. Rotation rates above $2\times$ are not possible with the model resolution used in this study due to numerical instability. This first set of simulations is referred to as free AHT simulations because radiation, and thus total AHT, can freely evolve. Radiative fluxes, and the resulting radiative temperature tendencies, are only a function of temperature since broadband optical depths are held constant and shortwave radiation is not absorbed in the atmosphere. A more detailed explanation of the radiation scheme can be found in Frierson et al. (2006). We run each simulation for 10 years. From inspection of time series of global-mean atmospheric temperature, surface temperature, and net surface flux (not shown) we conclude that these simulations reach equilibrium within about a year. To ensure that each has reached equilibrium, we use the last eight years of each 10-yr simulation for analysis. There is significant variation in maximum total AHT among these free AHT simulations: from 4.83 PW at $2\times$ to 8.72 PW at $1/16\times$ (Fig. 1). Due to symmetry across the equator, AHT results are only shown for the Northern Hemisphere. The variation in total AHT agrees well with previous studies that found an increase in AHT with decreasing rotation rate (e.g., Navarra and Boccaletti 2002; Vallis and Farneti 2009; Kaspi and Showman 2015; Wang et al. 2018), but the variation is larger in magnitude than that found in Wang et al. (2018). The large variation in total AHT shows the ability of AHT to change in GRaM, in contrast to a previous study that used a range of moisture contents and found little change in total AHT (Frierson et al. 2007).

In the second set of numerical experiments we employ a novel way to hold total AHT fixed while the planetary rotation rate is varied. We consider the same range of rotation rates as mentioned in the preceding paragraph, but set total AHT to that of $1 \times$ free AHT. We achieve this by prescribing, at every time step, radiative heating and cooling (the convergence and divergence of longwave fluxes) and surface radiative fluxes to the zonal-mean and time-mean values from the $1 \times$ free AHT simulation, symmetrized across the equator. This second set of simulations is referred to as fixed AHT simulations. As opposed to the free AHT simulations, in fixed AHT simulations the radiative temperature tendency is not a function of

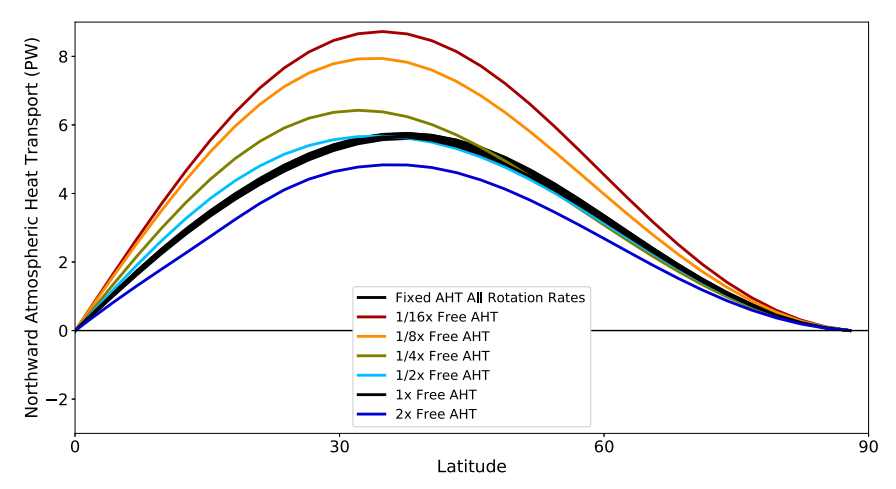


FIG. 1. Northward AHT for all simulations in the Northern Hemisphere. All *fixed AHT* simulations lie within the thick black line, and *free AHT* simulations are denoted by their respective colored line.

temperature, so temperatures and the radiative temperature tendency are no longer linked.

One consequence of specifying AHT in this way is that it removes the radiative damping that typically accompanies temperature fluctuations. This decoupling causes temperature drift and numerical instability in the highest atmospheric levels (above about 100 hPa) in some *fixed AHT* simulations. To remedy this we set radiative heating and cooling values (rad) to a combination of climatological (rad_clim) and model-calculated (rad_calc) values above the tropopause:

$$rad = [(1 - \kappa) \times rad_calc] + (\kappa \times rad_clim), \qquad (1)$$

where κ is set to 0.8 between the tropopause and 87 hPa and set to 0.3 above 87 hPa. Values of rad_calc are calculated identically to the manner used in *free AHT* simulations, and are only a function of temperature. It is not necessary to do this in the troposphere as there are sufficient mechanisms of adjustment (e.g., storms) to reach a stable equilibrium.

For fixed AHT simulations, we stipulate the magnitude of the total heat transported at each latitude, but not the mechanism that transports that heat. Importantly, both surface and atmospheric temperatures are allowed to change and can impact the dynamics of the system. In the troposphere, these temperature changes do not affect the radiative heating and cooling of the atmosphere and surface, thus removing any radiative-damping feedback to control these temperature changes. The fact that our simulations are still able to reach a stable equilibrium without a radiative-damping feedback shows the impressive compensatory ability of the atmosphere. This compensatory ability comes from atmospheric dynamics, which help smooth temperature anomalies. At the surface, the net flux must be equal to zero at equilibrium, as there is no ocean heat transport. Since the surface energy budget is a balance between radiative heating and turbulent energy loss, prescribing surface radiative fluxes to climatology means we are also prescribing the sum of the turbulent fluxes to climatology. Surface temperatures can still change due to a repartitioning of the sensible- and latent-heat fluxes via changes in near-surface winds and air-sea temperature and humidity gradients.

The fixed AHT simulations take much longer to reach statistical equilibrium since they do not have a radiative damping feedback in the troposphere. To account for this, we run each fixed AHT simulation for 30 years. We again assess equilibrium in each simulation by examining time series of global-mean atmospheric temperature, surface temperature, and net surface flux. The time it takes to reach equilibrium varies for each simulation, but for continuity we take the last eight years of 30-yr simulations as all experiments have reached equilibrium by this point. The result is a set of stable, fixed AHT simulations that show small differences in total AHT (typically less than 0.1 PW) from the $1 \times free\ AHT$ even as the planetary rotation rate is varied from $1/16 \times$ to $2 \times$ (Fig. 1).

These simulations provide an opportunity to separately probe the dynamic and radiative controls on AHT and its components. Our method for fixing the AHT of the system relies on setting the radiative fields to constant values. We can thus compare *fixed AHT* and *free AHT* simulations of the same rotation rate to explore the effects of radiative temperature tendencies. We can also explore the effects of rotation rate by comparing *fixed AHT* simulations of different rotation rates. This model framework also allows for a straightforward test of the hypothesis (e.g., Armour et al. 2019; Donohoe et al. 2020) that transient eddies are able to compensate for other changes to maintain invariant total AHT. In particular, we will examine how AHT components respond to create smoothly varying total AHT across different dynamical regimes without the added complexity of a change in total AHT.

3. Results

a. Effects of fixing radiation

We first consider how our methodology of fixing AHT by prescribing climatological radiative temperature tendencies may affect the climatology by comparing the $1 \times$ free AHT to

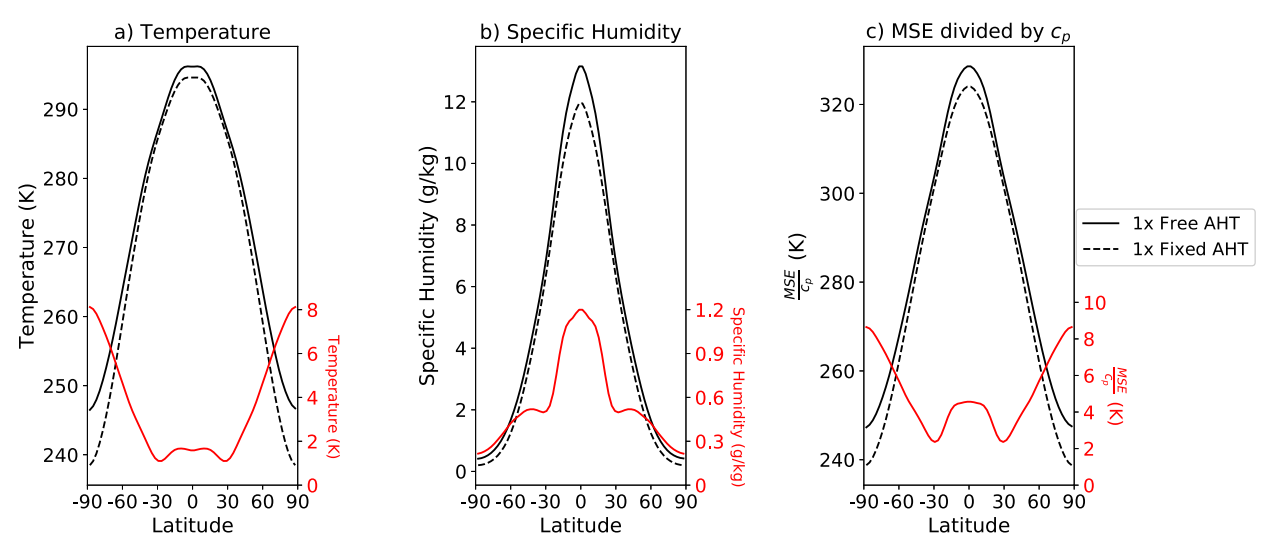


FIG. 2. Zonally averaged climatology of $1 \times$ fixed and *free AHT* simulations. (a) Surface temperatures, (b) near-surface specific humidity, and (c) near-surface MSE divided by c_p , the specific heat of air, for the $1 \times$ *free AHT* simulation (solid lines) and $1 \times$ *fixed AHT* simulation (dashed line) all symmetrized across the equator. Red lines are the difference between free and *fixed AHT* simulations.

the $1 \times$ fixed AHT simulations. Zonal-mean surface temperature changes are on the order of 1-2 K, except at high latitudes where changes are on the order of 5-10 K (Fig. 2a). Zonally averaged near-surface specific humidity changes less than 1 g kg⁻¹ everywhere except near the equator where changes reach 1.2 g kg⁻¹ (Fig. 2b). Moist static energy (MSE; i.e., the combination of sensible, latent, and geopotential energies) will become relevant when discussing AHT by eddies in section 3b. We convert MSE from joules per kilogram (J kg⁻¹) to more intuitive units of kelvin by dividing by c_p , the specific heat of air. MSE changes by less than 5 K, except near the poles where changes approach 10 K (Fig. 2c). There is a slight decrease in maximal zonal winds from 33 to 32 m s⁻¹ (see Fig. S1 in the online supplemental material). These changes are of minor consequence to AHT, with maximum northward AHT changing from 5.65 PW for $1 \times$ free AHT to 5.64 PW for $1 \times$ fixed AHT. The slight changes in AHT come from allowing some radiative temperature tendency changes above the troposphere. Changes in temperature, moisture, and circulation seen between the $1 \times$ free AHT and $1 \times$ fixed AHT simulations may be caused by these stratospheric radiative temperature tendencies. However, they could also be caused by our use of the time-mean climatology, rather than instantaneous, radiative temperature tendency profiles. Any nonlinearity, such as that between temperature and radiative tendency, can cause mean-state changes when time-mean climatology is used. This is similar to why cloud-locking experiments use instantaneous rather than time-mean values (e.g., Ceppi and Hartmann 2016). The changes to the mean state do not strongly affect AHT or atmospheric circulations patterns, which are the topic of this study. Moreover, to account for these small changes in the mean state, we take anomalies of fixed AHT simulations with respect to $1 \times$ fixed AHT and anomalies of free AHT simulations with respect to $1 \times$ free AHT.

b. AHT compensation mechanisms

Across our range of simulations, total AHT and its components vary significantly (Figs. 1 and 3). Despite these large variations, total AHT always varies smoothly with latitude in coordination with the radiative control on the climate system. Additionally, there are only small changes in the latitude of maximum total AHT, even as the magnitude of total AHT varies and the AHT components vary in latitudinal shape and magnitude. The lack of changes in the latitude of maximum total AHT is consistent with the hypothesis that the latitude of maximum total AHT is fixed by fundamental aspects of Earth's climate system, namely the meridional shape of absorbed solar radiation (Stone 1978).

To better understand what accounts for the differences in total AHT, it is necessary to look at individual AHT mechanisms. There is a large difference in total AHT between $1/16 \times$ fixed and 1/16× free AHT simulations (Fig. 3a). In both simulations, eddies provide only a small amount of AHT, while the MMC provides the bulk of AHT. The small role of eddies in AHT at slow rotation rates supports previous work (e.g., Del Genio and Suozzo 1987; Navarra and Boccaletti 2002; Kaspi and Showman 2015; Wang et al. 2018). Differences in AHT by the MMC can account for nearly all the difference in total AHT between 1/16× fixed and 1/16× free AHT simulations. At slow rotation rates such as 1/16×, the MMC is the compensating mechanism that helps satisfy radiative controls by creating smoothly varying total AHT. This is contrary to the hypothesis of previous work (Armour et al. 2019; Donohoe et al. 2020) that transient eddies are the primary compensating mechanism. While previous studies have noted that transient eddies play a minor role in time-mean AHT at slow rotation rates, this work builds on that to note that transient eddies are also less flexible than the MMC as an AHT mechanism at slower rotation rates.

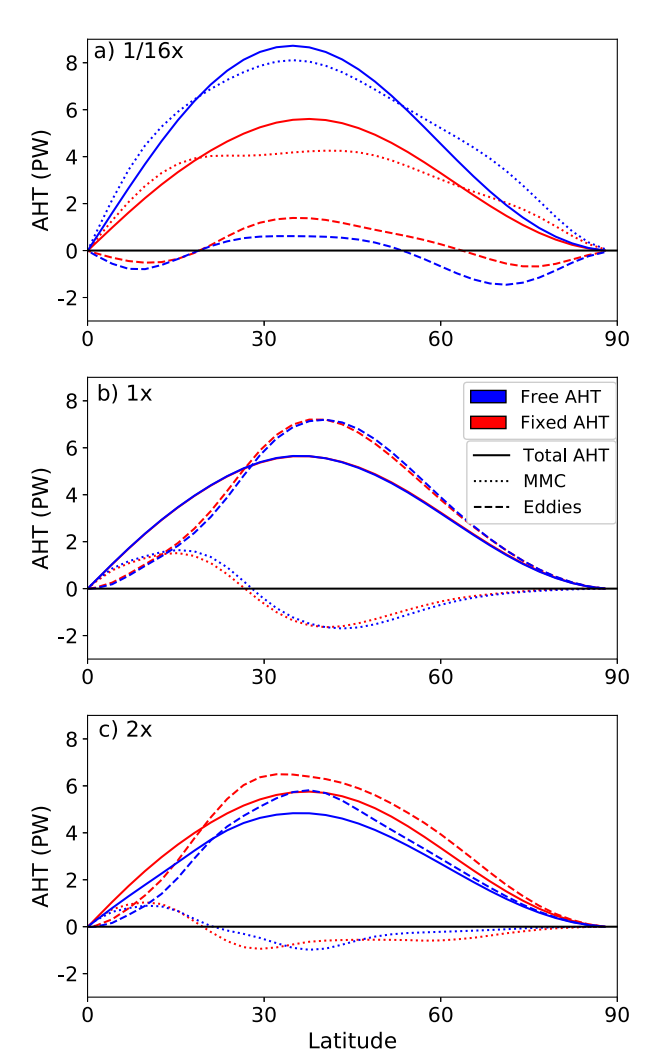


FIG. 3. Total northward AHT (solid) and its components, eddies (dashed), and MMC (dotted) in the Northern Hemisphere. *fixed AHT* simulations (red) and *free AHT* simulations (blue) are shown for a range of rotation rates, (a) $1/16\times$, (b) $1\times$, and (c) $2\times$.

The $2\times$ simulations differ from the $1/16\times$ simulations in several key ways. First, in the $2\times$ simulations, AHT is provided primarily by eddies while the MMC plays a minor role (Fig. 3c). Second, most of the difference in total AHT between $2\times$ fixed and $2\times$ free AHT simulations can be accounted for in differences in AHT by eddies. Thus, at higher rotation rates (between $1\times$ and $2\times$), eddies are indeed the compensating mechanism that maintains smoothly varying total AHT, consistent with the hypothesis of previous work (Armour et al. 2019; Donohoe et al. 2020).

These end member rotation rate experiments, $1/16\times$ and $2\times$, show that under different dynamical regimes either the MMC or eddies can dominate AHT adjustment. To better understand AHT across our range of planetary rotation rates, we examine each AHT component individually. Rotation rates between these two extremes are complicated by the fact that both the MMC and eddies play an important role in AHT

(Fig. S2). Due to this complication, results of the middle rotation rates are only discussed in relation to the end member rotation rate experiments.

c. Mean meridional circulation

1) ROTATION RATE INFLUENCE ON MMC AHT

We next isolate the effect of planetary rotation rate on AHT by the MMC by comparing the $1/16 \times fixed AHT$ and $1 \times fixed$ AHT simulations. We evaluate the mass-overturning, meridional streamfunction as a measure of the structure and strength of the MMC in each simulation (Fig. 4). The Hadley cell dominates AHT and mass transport by the MMC at slow rotation rates, and the Ferrel cell no longer forms in the 1/16× simulations. References to the MMC refer exclusively to the Hadley cell in the remainder of section 3c. Compared to the $1\times$ fixed AHT simulation, the 1/16× fixed AHT simulation has a Hadley cell that has a larger latitudinal extent (Figs. 4a,c) and is stronger, with maximum AHT by the MMC increasing from $1.6\,$ to 4.3 PW and mass transport increasing from 190 to 570 Sv $(1 \text{ Sy} \equiv 10^6 \text{ m}^3 \text{ s}^{-1})$ (Fig. 5). The changes in AHT by the MMC are smaller than those found in other work (Navarra and Boccaletti 2002; Kaspi and Showman 2015; Wang et al. 2018), but are similar to other work when we allow the radiation to respond (see the following section). The vertical extent of the Hadley cell circulation does not change significantly, while the subsiding branch broadens and becomes less vertical. It does not appear that changes to the shape of the Hadley cell subsiding branch are important for changes in heat or mass transport. In these fixed AHT simulations, when the radiative temperature tendency is kept constant while the rotation rate is slowed, there is a large increase in the latitudinal extent and strength of the Hadley cell, as can be seen in Figs. 4a and 5.

2) RADIATIVE TEMPERATURE TENDENCY INFLUENCE ON MMC AHT

To isolate the role of radiative temperature tendencies on AHT by the MMC we compare the $1/16 \times$ free AHT to $1/16 \times$ fixed AHT. The Hadley cells in both 1/16× simulations have similar latitudinal extent (Figs. 4a,b), but the strength of the mass transport has increased from 570 Sv for fixed AHT to 1200 Sv for free AHT (Figs. 4a,b). These results suggest that radiative tendency has an effect on Hadley cell strength, but not on Hadley cell latitudinal extent. Additionally, AHT by the MMC increases from 4.3 to 8.1 PW (Fig. 3a). Note that both of these values have increased by approximately a factor of 2. This scaling between mass and heat transport will be explored in a following section. AHT by the MMC between the $1 \times$ free AHT simulation and 1/16× free AHT simulation increases from 1.6 to 8.1 PW, which is similar to previous work that explored the influence of rotation rate on Hadley cell strength (Navarra and Boccaletti 2002; Kaspi and Showman 2015; Wang et al. 2018).

3) HADLEY CELL EXTENT

Various definitions of Hadley cell extent have been proposed [summarized in Levine and Schneider (2011)]. Building off of Walker and Schneider (2006), we define the extent of the

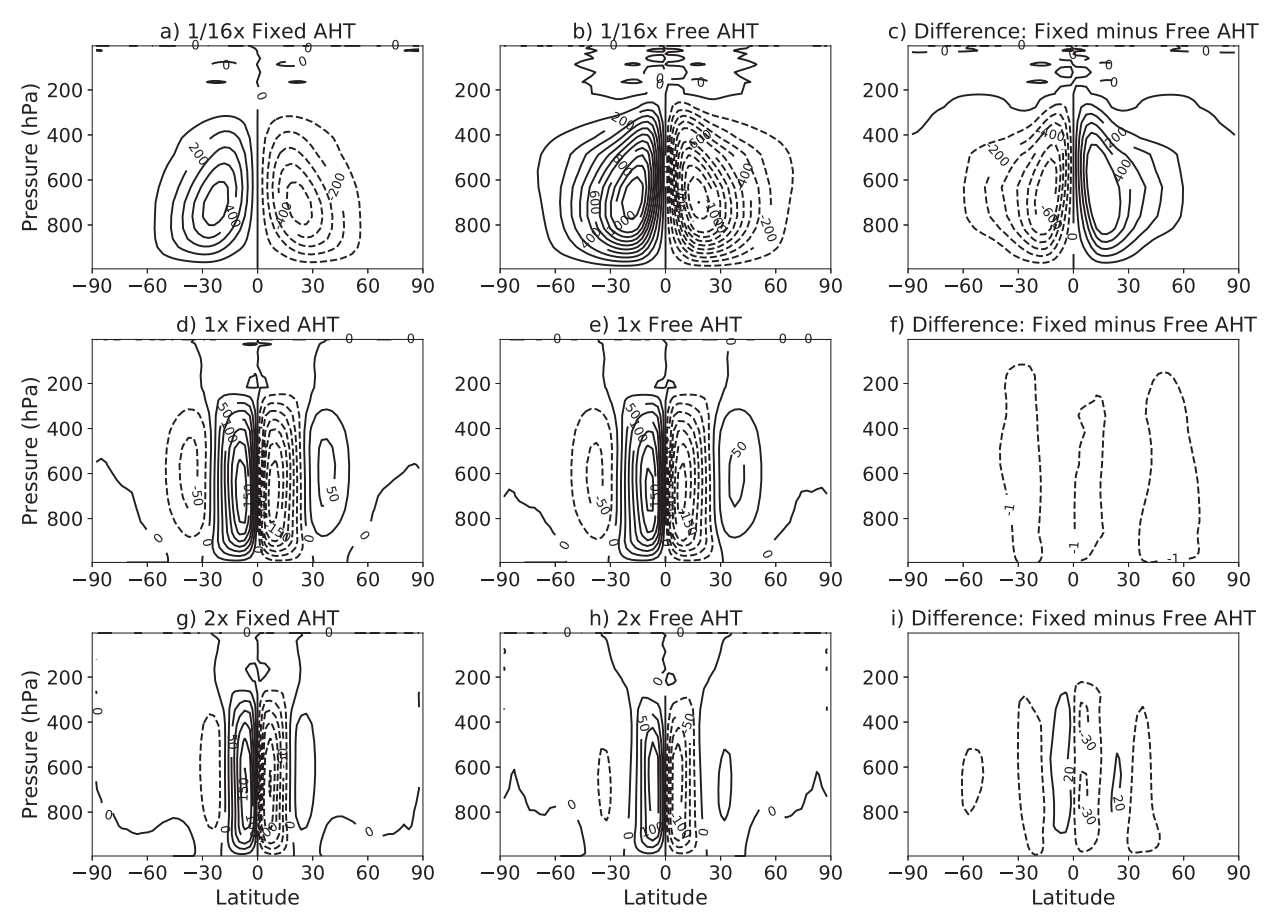


FIG. 4. Mass-overturning streamfunctions for (a) $1/16 \times$ fixed AHT, (b) $1/16 \times$ free AHT, (d) $1 \times$ fixed AHT, (e) $1 \times$ free AHT, (g) $2 \times$ fixed AHT, and (h) $2 \times$ free AHT. (c),(f),(i) The differences between fixed and free AHT simulations for the $1/16 \times$, $1 \times$, and $2 \times$, respectively. Contour intervals are 100 Sy for (a)–(c) and 25 Sy for (d)–(f).

Hadley cell as the latitude poleward of the mass-overturning streamfunction maximum where its value drops to 10% of its maximum, evaluated at the same level as the streamfunction maximum. This definition matches well with those based on surface winds or precipitation (not shown).

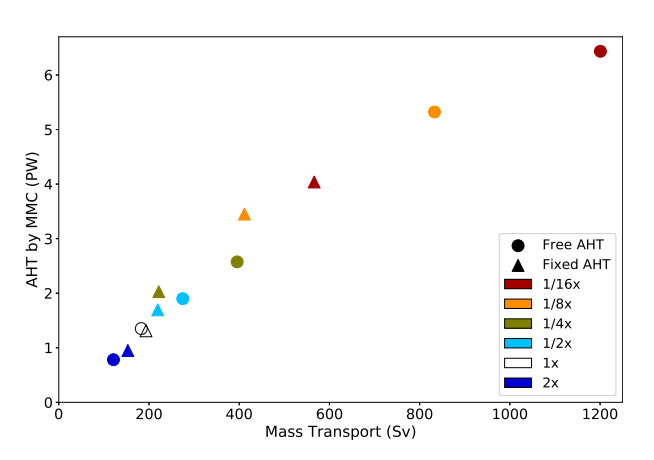


FIG. 5. Mass transport (Sv) vs AHT (PW) done by the Hadley cell. Both values are evaluated at the latitude of maximum mass-overturning streamfunction.

Across our range of simulations, there are substantial changes in the extent of the Hadley cell, from 18° to 66° latitude (Fig. 6). This range agrees well with previous studies that have explored the influence of rotation rate on Hadley cell extent

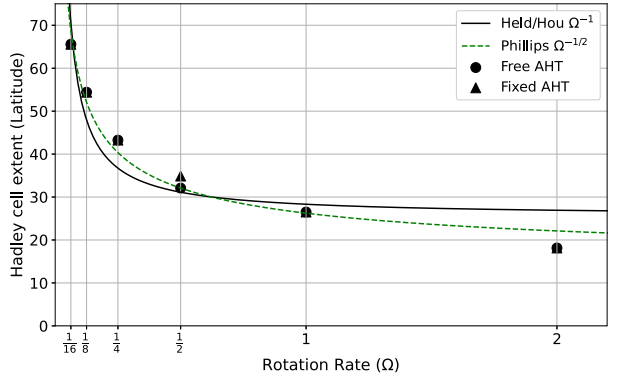


FIG. 6. Extent of the Hadley cell as a function of rotation rate. The extent is determined by the latitude at which the streamfunction has dropped to 10% of its maximum value. *fixed AHT* simulations (triangles) and *free AHT* simulations (circles) are shown. Prediction lines are $1/\Omega$ scaling (solid) as proposed by Held and Hou (1980), and the $1/\Omega^{1/2}$ (dashed green) from the Phillips (1954) two-layer model.

(e.g., Navarra and Boccaletti 2002; Kaspi and Showman 2015; Wang et al. 2018). Fixed and *free AHT* simulations of the same rotation rate have nearly identical latitudinal extents across the full range of our simulations. This suggests that, over this range of simulations, the extent of the Hadley cell is primarily determined by the dynamic control, the rotation rate, and that differences in radiative temperature tendencies have little effect on Hadley cell extent.

We compare these results to two existing theories of Hadley cell extent. The first is the inviscid axisymmetric theory developed by Held and Hou (1980). Assuming that the upper branch of the Hadley cell is angular momentum conserving, and that there is no net heating within the Hadley cell, this theory predicts that Hadley cell extent scales as Ω^{-1} . When fit to our data using nonlinear least squares minimization, the Ω^{-1} dependence predicts Hadley cell extent well, although it tends to overestimate the latitudinal extent at faster rotation rates (Fig. 6).

Other theories propose that the Hadley cell extends until the vertical shear becomes baroclinically unstable (e.g., Held 2000). Once again assuming that the upper branch of the Hadley cell is angular momentum conserving, the threshold for baroclinically unstable zonal winds yields a different scaling for the Hadley cell extent (e.g., Lu et al. 2007). Using the baroclinic instability criteria based on the two-layer model from Phillips (1954), this theory predicts the latitude of Hadley cell extent will scale as

latitude
$$\propto \left(\frac{NH_e}{\Omega a}\right)^{1/2}$$
, (2)

where N is the vertically averaged Brunt-Väisälä frequency, H_e is the local tropopause height, both evaluated at the edge of the Hadley cell, and a is Earth's radius. For our range of simulations, this scaling is dominated by the rotation rate Ω . That is, the Brunt-Väisälä frequency and local tropopause height, both taken to a one-half power, do not vary significantly across our range of simulations and cannot explain the Hadley cell extent changes (Fig. S3). The scaling of $\Omega^{-1/2}$ fit to our data using nonlinear least squares minimization predicts Hadley cell extent well (Fig. 6). These results suggest that the latitudinal extent of the Hadley cell is set primarily by planetary rotation rate and that radiative temperature tendencies, and their effects on factors such as tropopause height and static stability, play little role in setting Hadley cell extent over the range of rotation rates we have explored here. Other Hadley cell extent theories based on baroclinic instability, such as the criteria derived from the Eady growth rate (Lu et al. 2007), yield similar rotation rate scalings that also predict Hadley cell extent well for our simulations (not shown). Existing theories of Hadley cell extent do well because they depend strongly on rotation rate and secondarily on climate state variables.

4) Gross moist stability

We previously found that both Hadley cell mass transport and AHT approximately doubled from the $1/16 \times$ fixed AHT simulation to the $1/16 \times$ free AHT simulation. The linear scaling between Hadley cell AHT and mass transport seen in the $1/16 \times$ simulations holds more generally across the full

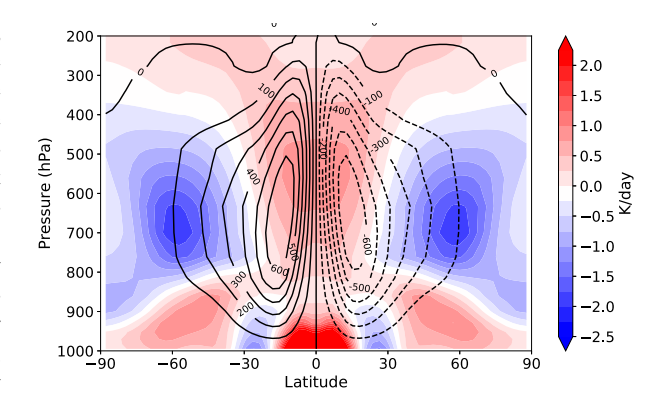


FIG. 7. Anomalies in mass overturning streamfunction (contours) and radiative cooling (filled contours), calculated from $1/16 \times free\ AHT$ simulation minus $1/16 \times fixed\ AHT$ simulation.

ensemble of free and fixed AHT rotation-rate experiments (Fig. 5). Held (2001) defined the ratio of AHT to mass transport in the Hadley cell as the gross moist stability (GMS) of the atmosphere: GMS = AHT by Hadley cell divided by mass transport. In conceptual terms, if the Hadley cell mass transports were confined to infinitely thin layers in the upper and lower branches, then the GMS would equal the equivalent potential temperature contrast between the upper and lower branches. More generally, GMS represents the mass-flux difference weighted in equivalent potential temperature between equatorward and poleward moving air (Back and Bretherton 2006). The near-linear slope between AHT and mass transport by the Hadley cell in Fig. 5 implies that GMS is approximately constant for all simulations. This is confirmed by vertical gradients of MSE (not shown), which are nearly invariant across all simulations. This does not suggest that this principle holds in our current climate, where past work (Walker and Schneider 2006) has shown GMS changes can be important for understanding changes in Hadley cell mass transport. However, for our range of simulations, in which the Hadley cell mass transport changes sixfold, changes in AHT by the MMC are driven by changes in mass transport, rather than by GMS changes.

5) DRIVERS OF HADLEY CELL DIFFERENCES

The above analysis shows that while planetary rotation rate alone can predict Hadley cell extent, heat and mass transport are determined by both dynamic and radiative controls. For fixed and *free AHT* simulations of a given rotation rate, differences in transport must be due to radiative effects. Specifically, the differences between fixed and *free AHT* simulations can be well explained by differences in radiative heating and cooling within the Hadley cell.

The effects of radiative anomalies are most clearly seen with the $1/16\times$ simulations in Fig. 7. The Hadley cells in both the $1/16\times$ fixed and $1/16\times$ free AHT simulations have a larger latitudinal extent and are stronger in magnitude than their respective $1\times$ simulations because of the slowed rotation rate. These dynamically forced changes to circulation patterns create different temperature profiles compared to $1\times$ simulations.

In the $1/16 \times fixed\ AHT$ simulation these temperature changes create no radiative changes in the troposphere. In the $1/16 \times free\ AHT$ case, the temperature changes do create radiative changes. The most important radiative changes appear to be located in the ascending and descending branches of the Hadley cell. There is stronger radiative cooling in the subsiding branch that is thermodynamically balanced by adiabatic descent and creates a stronger Hadley cell circulation, consistent with previous work (Trenberth and Stepaniak 2003; Merlis 2015). Similarly, the deep tropics in the $1/16 \times free\ AHT$ simulation cool relative to the $1 \times free\ AHT$ simulation due to enhanced export by AHT, inducing radiative heating anomalies in $1/16 \times free\ AHT$ simulation (Fig. 7) that are balanced by adiabatic ascent (i.e., strengthening of the Hadley cell).

These results illustrate a coupling between dynamical and radiative changes. Planetary rotation rate changes strengthen and increase the width of the Hadley cell in the 1/16× simulations, leading to cooling in the ascending branch and warming in the descending branch. In turn, this enhances radiative heating in the ascending branch and radiative cooling in the descending branch when radiation is allowed to respond in the $1/16 \times$ free AHT simulation. These radiative anomalies further strengthen the Hadley cell, but do not change its width. This coupling cannot be seen in AHT frameworks where dynamic and energetic constraints operate simultaneously, perhaps leading to the impression that energetic constraints control AHT (e.g., Armour et al. 2019; Donohoe et al. 2020) when in fact changes in radiation are also influenced by changes in circulation (e.g., Merlis 2015). The idea of coupled dynamic and radiative constraints also applies to the other slower rotation rates (Fig. S4). At rotation rates of $1 \times$ and faster, where the MMC contributes a small portion of AHT, this coupling is less apparent and can behave differently. In the $2 \times$ simulations the coupling between dynamics and radiation works in reverse to weaken the Hadley cell (Fig. 5). The 2× fixed AHT simulation has a slightly stronger Hadley cell than the $2 \times$ free AHT simulation. The difference in strength is due to enhanced radiative cooling in the ascending branch of the Hadley cell in the $2 \times$ free AHT, compared to that of the $2 \times$ fixed AHT simulation, that occurs due to diminished AHT out of the tropics (not shown).

d. Transient eddies

AHT by eddies makes up an increasing fraction of total AHT at faster rotation rates, and dominates total AHT in the $2\times$ simulations (Fig. 3c). We focus on $1/2\times$, $1\times$, and $2\times$ simulations to explore how rotation rate and radiative temperature tendencies affect AHT by eddies. The $1/2\times$ fixed AHT and $1/2\times$ free AHT simulations both have maximums of 7.0 PW of AHT by eddies. Both $1\times$ fixed and $1\times$ free AHT simulations have maximums of 7.2 PW of AHT by eddies. The $2\times$ simulations exhibit substantial differences in maximum AHT by eddies with fixed and free AHT simulations having maximums of 6.5 and 5.8 PW of AHT by eddies, respectively. AHT by eddies is not constant between fixed AHT simulations of different rotation rates. The Ferrel cell makes up the difference between eddy AHT at rotation rates equal to and above $1/2\times$, to result in the same total AHT in the midlatitudes. We find

that the magnitude of Ferrel cell AHT is nearly identical for fixed and *free AHT* simulations of a given rotation rate and scales with the convergence of eddy AHT (not shown), as expected from previous work (e.g., Salustri and Stone 1983).

1) ROTATION RATE INFLUENCE ON TRANSIENT EDDY AHT

We evaluate the influence of rotation rate on AHT by eddies by comparing the $1/2 \times fixed AHT$, $1 \times fixed AHT$, and $2 \times fixed$ AHT simulations. These simulations have maximums of 7.0, 7.2, and 6.5 PW of AHT by eddies respectively. Meridional gradients in MSE, eddy kinetic energy, and the vertical structure of eddies all play an integral role in eddy AHT (e.g., Lorenz 1955; Stone 1972). In this work we focus on the role of meridional gradients in MSE, but note that there are not significant changes in the vertical structure of eddies among these simulations. To quantify the meridional MSE gradient we use the near-surface MSE difference between equatorial (0°-30°) and polar (60°-90°) regions and divide by c_p to convert to intuitive units of kelvin. Qualitatively similar results are found using alternative latitude bands and vertical levels, or local gradients in MSE averaged over the midlatitude region. The equator-pole MSE difference increases for the 2× fixed AHT simulation, 88 K, and decreases for the 1/2× fixed AHT simulation, 64 K, compared to the $1 \times$ fixed AHT simulation, 69 K (Fig. 8b).

To connect changes in meridional MSE differences to changes in AHT by eddies, we use the linear, downgradient diffusion principle that has been shown to accurately predict AHT and its changes (Flannery 1984; Roe et al. 2015; Bonan et al. 2018; Merlis and Henry 2018; Siler et al. 2018; Armour et al. 2019). The assumption that energy is transported, diffusively, down the MSE gradient works remarkably well at all latitudes in both observations and comprehensive GCMs (Armour et al. 2019), despite theory that suggests only the extratropical region, dominated by transient eddies, should behave in this way (Held 1999). Following Liu et al. (2017), we diagnose the effective diffusivity of the atmosphere $D_{\rm eff}$ from

AHT =
$$-2\pi \cos(\theta) \frac{p_s}{g} D_{\text{eff}}(\theta) \frac{dh}{d\theta}$$
, (3)

where $p_s g^{-1}$ is the mass per unit area (assumed to be a constant of $10^4 \,\mathrm{kg}\,\mathrm{m}^{-2}$), D_{eff} is the effective diffusivity as a function of latitude, and h is the zonally averaged near-surface MSE. We average the resulting D_{eff} values in the midlatitude, transient-eddy dominated region, which we define as the edge of the Hadley cell to 30° poleward of that latitude.

Compared to the $1\times$ fixed AHT simulation, $D_{\rm eff}$ decreases for the $2\times$ fixed AHT simulation and increases for the $1/2\times$ fixed AHT simulation (Table 1), suggesting that $D_{\rm eff}$ depends on rotation rate. The differences in $D_{\rm eff}$ are not linear with rotation rate, with the increase in $D_{\rm eff}$ for the $1/2\times$ fixed AHT simulation being smaller in magnitude than the decrease for the $2\times$ fixed AHT simulation.

Combining the ideas of effective diffusivity and meridional MSE differences provides a simple way to interpret changes in AHT by eddies. In *fixed AHT* simulations where AHT by

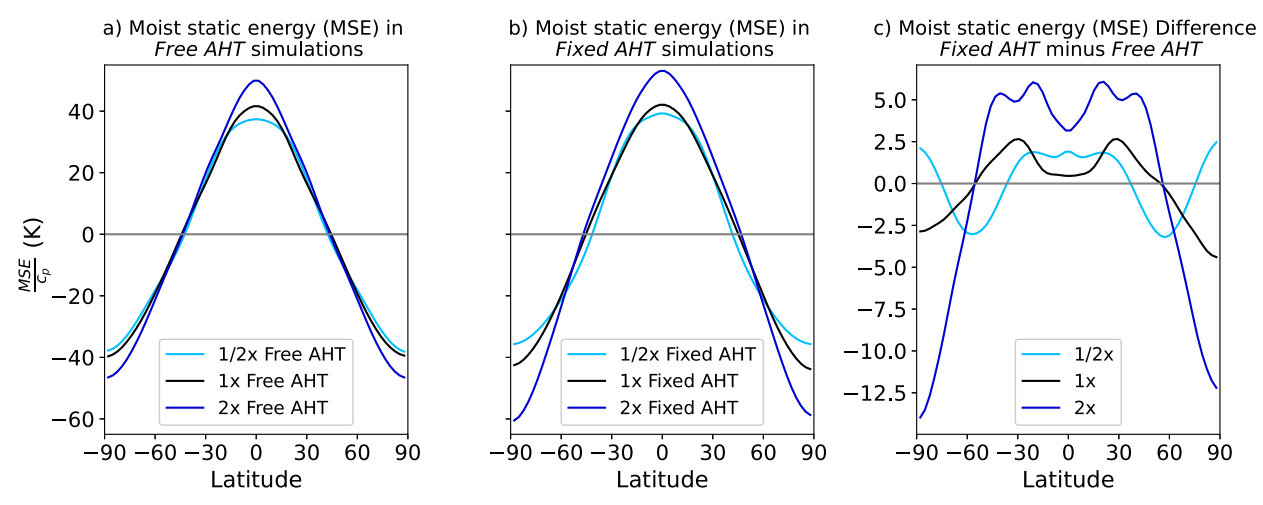


FIG. 8. Zonally averaged near-surface moist static energy anomalies from the global mean divided by c_p for (a) free AHT simulations of $1/2 \times$, $1 \times$, and $2 \times$; (b) fixed AHT simulations of $1/2 \times$, $1 \times$, and $2 \times$; and (c) the difference between fixed and free AHT simulations.

eddies dominates total AHT ($1/2\times$ and faster), the changes in $D_{\rm eff}$ must be balanced by changes in meridional MSE difference to maintain near-constant total AHT. This explains why changes in $D_{\rm eff}$ and the meridional MSE difference are of opposite sign in both the $1/2\times$ fixed AHT and $2\times$ fixed AHT simulations.

2) RADIATIVE TEMPERATURE TENDENCY INFLUENCE ON TRANSIENT EDDY AHT

We evaluate the role of radiative temperature tendency on eddy AHT by comparing the $1/2\times$, $1\times$, and $2\times$ fixed AHT simulations to their corresponding free AHT simulations. These simulations have maximums of 7.0, 7.2, and 5.8 PW of AHT by eddies respectively. The $2 \times$ free AHT meridional MSE difference, 75 K, has decreased in magnitude compared to the 2× fixed AHT simulation, 88 K, but is still larger than the MSE difference, 65 K, of its control the 1× free AHT simulation (Fig. 8a). The MSE difference in the $1/2 \times$ free AHT simulation, 62 K, is nearly unchanged compared to the $1/2\times$ fixed AHT simulation, 64 K, both of which are less than their 1× controls. These changes suggest that the equator–pole MSE difference is determined by both rotation rate and radiative temperature tendency for 2× simulations, but only by the rotation rate for 1/2× simulations. The lack of influence by radiative temperature tendency in the $1/2 \times$ simulations is likely due to the very small amplitude of changes in midlatitude

TABLE 1. Effective diffusivity $D_{\rm eff}$ (m² s⁻¹ × 10⁶) at the near surface averaged between the edge of the Hadley cell and 30° poleward of that point for $1/2 \times$, 1×, and 2× simulations.

Rotation rate	Free AHT	Fixed AHT
1/2×	1.68	1.64
1×	1.61	1.50
$2\times$	1.09	1.24

radiative cooling between $1/2 \times fixed\ AHT$ and $1/2 \times free\ AHT$ simulations (Table 2).

The $D_{\rm eff}$ values are similar between fixed and free AHT simulations of a given rotation rate (Table 1). This suggests that $D_{\rm eff}$ is solely controlled by rotation rate for eddydominated AHT regimes. The value of $D_{\rm eff}$ is not solely controlled by dynamics at slower rotation rates, where there are significant changes in D_{eff} for fixed and free AHT simulations of a given rotation rate (Fig. S5). We do not find the near-linear relation between $D_{\rm eff}$ and length and velocity scalings from eddy mixing length theory as in Liu et al. (2017) (Fig. S5). Additionally, this entire linear, downgradient diffusion of MSE appears to break down at slower rotation rates where values of $D_{\rm eff}$ vary erratically with latitude and attempts to accurately predict AHT using this downgradient diffusive framework fail (not shown). This failure is likely due to the reliance of this theory on eddies, which have a diminishing role at slow rotation rates.

3) DRIVERS OF TRANSIENT EDDY AHT DIFFERENCES

There are only small changes in eddy AHT between $1/2 \times$ fixed and *free AHT* simulations, as both have a maximum northward AHT by eddies of 7.0 PW (Fig. S2c). The most pronounced differences between eddy AHT in free versus *fixed AHT* simulations occur for the $2 \times$ simulations (6.5 PW in $2 \times$

TABLE 2. Vertically and zonally averaged radiative cooling (K day $^{-1}$), in the middle and high latitudes of faster rotation rates. All quantities are averages from 300 to 950 hPa and poleward of 30° latitude for $1/2 \times$, $1 \times$, and $2 \times$ simulations (K day $^{-1}$). Fixed AHT simulations are nearly identical by experimental design.

Rotation rate	Free AHT	Fixed AHT
1/2×	-1.75	-1.75
1×	-1.76	-1.76
$2\times$	-1.61	-1.76

fixed AHT and 5.8 PW in $2 \times$ free AHT) and we focus our analysis here on these two experiments. The differences in AHT in these $2 \times$ simulations come from changes in meridional MSE differences, as decreases in $D_{\rm eff}$, relative to the $1 \times$ simulations, are similar (Table 1).

In the $2\times$ fixed AHT simulation the decrease in $D_{\rm eff}$, compared to the $1\times$ fixed AHT simulation, is countered by an increase in the meridional MSE difference to maintain constant total AHT. If there were perfect compensation between $D_{\rm eff}$ and the meridional MSE difference, and all AHT was done by eddies, then AHT by eddies would not change between the $1\times$ fixed AHT and $2\times$ fixed AHT simulations. However, eddy AHT is not constant between the $1\times$ fixed AHT and $2\times$ fixed AHT simulations due to a change in magnitude of the maximum Ferrel cell AHT from -1.7 to -1.1 PW respectively, and due to shifts in the latitudinal structure of the eddies and MMCs (Figs. 3b,c). As a result, the compensation between $D_{\rm eff}$ and meridional MSE difference is good, but imperfect, at maintaining the same magnitude of eddy AHT.

The $2 \times$ free AHT simulation has even more imperfect compensation between $D_{\rm eff}$ and the meridional MSE difference than the $2 \times fixed AHT$ simulation because of radiative temperature tendency effects. The worse compensation in the 2× free AHT simulation comes from a smaller meridional MSE difference than the $2 \times fixed AHT$ simulation, since values of $D_{\rm eff}$ are similar. To understand why there are differences in meridional MSE difference, it is informative to think through the evolution of the $2 \times$ fixed AHT simulation from spin-up to equilibrium. When the rotation rate is increased to $2\times$, D_{eff} decreases, which results in less total AHT. The decrease in total AHT results in cooling in the extratropical region, and a larger meridional MSE difference. The optical depth is held constant in this modeling framework, so a decrease in extratropical temperatures results in less radiation to space (Table 2). This decrease in outgoing radiation allows extratropical temperatures to warm and partially rebound toward the original values from the 1× free AHT control simulation. This radiatively induced warming decreases the meridional MSE difference in the $2 \times$ free AHT compared to the $2 \times fixed AHT$ simulation. Compared to the $2 \times fixed AHT$ simulation, the 2× free AHT simulation has poorer compensation between $D_{\rm eff}$ and the meridional MSE difference resulting in less eddy AHT.

The meridional MSE difference is partially dynamically controlled (both $2\times$ simulations have larger MSE differences then their $1\times$ controls) and partially radiatively controlled (the MSE differences vary between $2\times$ *fixed AHT* and $2\times$ *free AHT*). These same principles do not apply to the simulations with rotation rates of $1/2\times$ and slower where there are either only small radiative cooling differences between fixed and *free AHT* simulations (Table 2) or eddies play a minor role in AHT.

4. Summary and discussion

Due to the difficulty of separating the relative influences of dynamical and radiative controls on AHT, previous research has studied their combined, simultaneous influence on AHT within observations and comprehensive GCMs. This work employed a novel, idealized modeling framework that permits an assessment of the individual contributions from each control, and their interaction, on AHT.

Individual aspects of AHT are controlled in different ways by radiation and dynamics. The planetary rotation rate (the dynamical control in this study) strongly controls Hadley cell extent at all rotation rates, while the radiative temperature tendency (the radiative control in this study) plays little role in the Hadley cell extent in these simulations. This confirms previous work that finds rotation rate has a significant influence over Hadley cell extent (e.g., Del Genio and Suozzo 1987; Navarra and Boccaletti 2002; Kaspi and Showman 2015; Guendelman and Kaspi 2019; Hill et al. 2019; Singh 2019). The planetary rotation rate also controls the effective diffusivity $D_{\rm eff}$ at rotation rates equal to or faster than 1/2×. Both the planetary rotation rate and radiative temperature tendency (the radiative control in this study) have influence over the strength of the Hadley cell and the magnitude of MSE meridional differences. The gross moist stability of the tropical atmosphere is nearly invariant across the wide range of circulations probed in our study and, thus, the AHT changes in the Hadley cell are predominantly a consequence of its mass transport. Both radiative temperature tendencies and the planetary rotation rate have influence on the mass transport of the Hadley cell in MMC-dominated regimes. A dynamical change of rotation rate from $1 \times fixed AHT$ to $1/16 \times fixed AHT$ produces increases of 2.9 times in mass transport and 2.5 times in AHT by the MMC. The radiative temperature tendency shift from 1/16× fixed AHT to 1/16× free AHT produces similar magnitude changes with increases of 2.1 times in mass transport and 1.9 times in AHT by the MMC. Both radiation and rotation rate changes alter the equator-pole MSE difference. The rotation rate increases this MSE difference by 28%, from $1 \times$ fixed AHT to $2 \times$ fixed AHT, while the radiative temperature tendencies decrease the MSE difference by 15%, from $2 \times$ *fixed AHT* to $2 \times$ *free AHT*.

The radiative and dynamic controls do not always operate independently. We have found a direct coupling between the radiative and dynamic controls in determining the strength of the Hadley cell in the $1/16 \times$ simulations. This coupling allows for enhanced strengthening to occur, creating an extremely strong Hadley cell that transports 6.2 times more mass than model climatology. Specifically, in the 1/16× free AHT simulation, rotation rate-induced circulation changes create anomalous radiative cooling, which reinforces and strengthens the circulation changes. The radiative and dynamic controls do not always reinforce each other. In the $2 \times free AHT$ simulation an increased rotation rate decreases the efficiency of eddy AHT, which works to increase the meridional MSE difference. Meanwhile, radiative temperature tendencies decrease the meridional MSE difference through diminished radiative cooling in the extratropics. Previous AHT frameworks have not been able to describe the specific mechanisms of these couplings.

The hypothesis that transient eddies are the compensating mechanism creating smoothly varying AHT at all latitudes (Armour et al. 2019; Donohoe et al. 2020) does not hold in climates where AHT is dominated by the MMC, but does apply

in climates with similar rotation rates to Earth's where eddies play a more important role. This hypothesis is based on the idea that transient eddies are the most efficient AHT component to smooth atmospheric heating anomalies, which results in smoothly varying AHT (Farneti and Vallis 2013; Donohoe et al. 2020). While this may hold true for Earth-like rotation rates, at slow rotation rates eddies provide a small amount of AHT in the time mean, confirming previous work (e.g., Del Genio and Suozzo 1987; Navarra and Boccaletti 2002; Kaspi and Showman 2015; Wang et al. 2018). As a result, the ability of transient eddies to smooth these heating anomalies is reduced. In these slow-rotation regimes, the Hadley cell dominates AHT, and appears fully capable of smoothing atmospheric heating anomalies that do occur. This suggests the AHT system can adjust in more ways than previously thought.

Acknowledgments. We thank Dennis Hartmann and Brian Green for helpful conversation about Hadley cell theory. We would also like to thank two anonymous reviewers for their helpful comments. DMWF was supported by National Science Foundation Award AGS-1665247. AD was funded by the National Science Foundation Paleo Perspective on Climate Change (P2C2) Grant AGS-1702827. We acknowledge support for KCA from National Science Foundation Award AGS-1752796. We also acknowledge support for TC, KCA, AD, and GHR from National Science Foundation Award CLD-2019647.

Data availability statement. The model data for this study are stored on University of Washington servers and can be made available upon reasonable request to the authors.

REFERENCES

- Armour, K. C., N. Siler, A. Donohoe, and G. H. Roe, 2019: Meridional atmospheric heat transport constrained by energetics and mediated by large-scale diffusion. *J. Climate*, 32, 3655–3680, https://doi.org/10.1175/JCLI-D-18-0563.1.
- Back, L., and C. Bretherton, 2006: Geographic variability in the export of moist static energy and vertical motion profiles in the tropical Pacific. *Geophys. Res. Lett.*, 33, L17810, https:// doi.org/10.1029/2006GL026672.
- Bonan, D., K. Armour, G. Roe, N. Siler, and N. Feldl, 2018: Sources of uncertainty in the meridional pattern of climate change. *Geophys. Res. Lett.*, 45, 9131–9140, https://doi.org/ 10.1029/2018GL079429.
- Brayshaw, D. J., B. Hoskins, and M. Blackburn, 2009: The basic ingredients of the North Atlantic storm track. Part I: Land–sea contrast and orography. J. Atmos. Sci., 66, 2539–2558, https:// doi.org/10.1175/2009JAS3078.1.
- Ceppi, P., and D. L. Hartmann, 2016: Clouds and the atmospheric circulation response to warming. *J. Climate*, 29, 783–799, https://doi.org/10.1175/JCLI-D-15-0394.1.
- Del Genio, A. D., and R. J. Suozzo, 1987: A comparative study of rapidly and slowly rotating dynamical regimes in a terrestrial general circulation model. *J. Atmos. Sci.*, 44, 973–986, https://doi.org/ 10.1175/1520-0469(1987)044<0973:ACSORA>2.0.CO;2.
- Donohoe, A., K. C. Armour, G. H. Roe, D. S. Battisti, and L. Hahn, 2020: The partitioning of meridional heat transport from the last glacial maximum to CO₂ quadrupling in coupled climate models. *J. Climate*, 33, 4141–4165, https://doi.org/10.1175/JCLI-D-19-0797.1.

- Farneti, R., and G. K. Vallis, 2013: Meridional energy transport in the coupled atmosphere–ocean system: Compensation and partitioning. *J. Climate*, **26**, 7151–7166, https://doi.org/10.1175/JCLI-D-12-00133.1.
- Flannery, B. P., 1984: Energy balance models incorporating transport of thermal and latent energy. *J. Atmos. Sci.*, **41**, 414–421, https://doi.org/10.1175/1520-0469(1984)041<0414:EBMITO>2.0.CO;2.
- Frierson, D. M., 2007: The dynamics of idealized convection schemes and their effect on the zonally averaged tropical circulation. J. Atmos. Sci., 64, 1959–1976, https://doi.org/10.1175/ JAS3935.1.
- —, I. M. Held, and P. Zurita-Gotor, 2006: A gray-radiation aquaplanet moist GCM. Part I: Static stability and eddy scale. J. Atmos. Sci., 63, 2548–2566, https://doi.org/10.1175/JAS3753.1.
- —, —, and —, 2007: A gray-radiation aquaplanet moist GCM. Part II: Energy transports in altered climates. *J. Atmos. Sci.*, **64**, 1680–1693, https://doi.org/10.1175/JAS3913.1.
- Guendelman, I., and Y. Kaspi, 2019: Atmospheric dynamics on terrestrial planets: The seasonal response to changes in orbital, rotational, and radiative timescales. *Astrophys. J.*, 881, 67, https://doi.org/10.3847/1538-4357/ab2a06.
- Held, I. M., 1999: The macroturbulence of the troposphere. *Tellus*, **51**, 59–70, https://doi.org/10.3402/tellusb.v51i1.16260.
- —, 2000: The general circulation of the atmosphere. Proc. 2000 Program in Geophysical Fluid Dynamics, Woods Hole, MA, Woods Hole Oceanographic Institute, 1–54.
- —, 2001: The partitioning of the poleward energy transport between the tropical ocean and atmosphere. J. Atmos. Sci., 58, 943–948, https://doi.org/10.1175/1520-0469(2001)058<0943:TPOTPE>2.0.CO:2.
- —, and A. Y. Hou, 1980: Nonlinear axially symmetric circulations in a nearly inviscid atmosphere. J. Atmos. Sci., 37, 515–533, https:// doi.org/10.1175/1520-0469(1980)037<0515:NASCIA>2.0.CO;2.
- —, and B. J. Soden, 2006: Robust responses of the hydrological cycle to global warming. *J. Climate*, **19**, 5686–5699, https:// doi.org/10.1175/JCLI3990.1.
- Hill, S. A., S. Bordoni, and J. L. Mitchell, 2019: Axisymmetric constraints on cross-equatorial Hadley cell extent. J. Atmos. Sci., 76, 1547–1564, https://doi.org/10.1175/JAS-D-18-0306.1.
- Holton, J. R., and G. J. Hakim, 2013: An Introduction to Dynamic Meteorology. 5th ed. Academic Press, 532 pp.
- Hunt, B., 1979: The influence of the Earth's rotation rate on the general circulation of the atmosphere. *J. Atmos. Sci.*, **36**, 1392–1408, https://doi.org/10.1175/1520-0469(1979)036<1392:TIOTER>2.0.CO;2.
- Kaspi, Y., and T. Schneider, 2013: The role of stationary eddies in shaping midlatitude storm tracks. J. Atmos. Sci., 70, 2596– 2613, https://doi.org/10.1175/JAS-D-12-082.1.
- —, and A. P. Showman, 2015: Atmospheric dynamics of terrestrial exoplanets over a wide range of orbital and atmospheric parameters. *Astrophys. J.*, 804, 60, https://doi.org/10.1088/0004-637X/804/1/60.
- Levine, X. J., and T. Schneider, 2011: Response of the Hadley circulation to climate change in an aquaplanet GCM coupled to a simple representation of ocean heat transport. *J. Atmos. Sci.*, **68**, 769–783, https://doi.org/10.1175/2010JAS3553.1.
- Liu, X., D. S. Battisti, and G. H. Roe, 2017: The effect of cloud cover on the meridional heat transport: Lessons from variable rotation experiments. *J. Climate*, 30, 7465–7479, https://doi.org/ 10.1175/JCLI-D-16-0745.1.
- Lorenz, E. N., 1955: Available potential energy and the maintenance of the general circulation. *Tellus*, 7, 157–167, https:// doi.org/10.3402/tellusa.v7i2.8796.
- Lu, J., G. A. Vecchi, and T. Reichler, 2007: Expansion of the Hadley cell under global warming. *Geophys. Res. Lett.*, 34, L06805, https://doi.org/10.1029/2006GL028443.

- Merlis, T. M., 2015: Direct weakening of tropical circulations from masked CO₂ radiative forcing. *Proc. Natl. Acad. Sci. USA*, 112, 13 167–13 171, https://doi.org/10.1073/pnas.1508268112.
- —, and M. Henry, 2018: Simple estimates of polar amplification in moist diffusive energy balance models. *J. Climate*, 31, 5811– 5824, https://doi.org/10.1175/JCLI-D-17-0578.1.
- Navarra, A., and G. Boccaletti, 2002: Numerical general circulation experiments of sensitivity to Earth rotation rate. *Climate Dyn.*, **19**, 467–483, https://doi.org/10.1007/s00382-002-0238-8.
- Phillips, N. A., 1954: Energy transformations and meridional circulations associated with simple baroclinic waves in a two-level, quasi-geostrophic model. *Tellus*, 6, 274–286, https://doi.org/10.3402/tellusa.v6i3.8734.
- Pierrehumbert, R. T., 2010: *Principles of Planetary Climate*. Cambridge University Press, 679 pp.
- Roe, G. H., N. Feldl, K. C. Armour, Y.-T. Hwang, and D. M. Frierson, 2015: The remote impacts of climate feedbacks on regional climate predictability. *Nat. Geosci.*, 8, 135–139, https://doi.org/10.1038/ngeo2346.
- Salustri, G., and P. H. Stone, 1983: A diagnostic study of the forcing of the Ferrel cell by eddies, with latent heat effects included. *J. Atmos. Sci.*, **40**, 1101–1109, https://doi.org/10.1175/1520-0469(1983)040<1101:ADSOTF>2.0.CO;2.
- Saulière, J., D. J. Brayshaw, B. Hoskins, and M. Blackburn, 2012: Further investigation of the impact of idealized continents and SST distributions on the Northern Hemisphere storm tracks. *J. Atmos. Sci.*, 69, 840–856, https://doi.org/10.1175/JAS-D-11-0113.1.
- Siler, N., G. H. Roe, and K. C. Armour, 2018: Insights into the zonal-mean response of the hydrologic cycle to global warming from a diffusive energy balance model. *J. Climate*, 31, 7481–7493, https://doi.org/10.1175/JCLI-D-18-0081.1.

- Singh, M. S., 2019: Limits on the extent of the solsticial Hadley cell: The role of planetary rotation. *J. Atmos. Sci.*, **76**, 1989–2004, https://doi.org/10.1175/JAS-D-18-0341.1.
- Stone, P. H., 1972: A simplified radiative-dynamical model for the static stability of rotating atmospheres. *J. Atmos. Sci.*, **29**, 405–418, https://doi.org/10.1175/1520-0469(1972)029<0405: ASRDMF>2.0.CO;2.
- —, 1978: Constraints on dynamical transports of energy on a spherical planet. *Dyn. Atmos. Oceans*, 2, 123–139, https:// doi.org/10.1016/0377-0265(78)90006-4.
- Trenberth, K. E., and D. P. Stepaniak, 2003: Seamless poleward atmospheric energy transports and implications for the Hadley circulation. *J. Climate*, **16**, 3706–3722, https://doi.org/10.1175/1520-0442(2003)016<3706:SPAETA>2.0.CO;2.
- Vallis, G. K., and R. Farneti, 2009: Meridional energy transport in the coupled atmosphere–ocean system: Scaling and numerical experiments. *Quart. J. Roy. Meteor. Soc.*, **135**, 1643–1660, https://doi.org/10.1002/qj.498.
- Walker, C. C., and T. Schneider, 2006: Eddy influences on Hadley circulations: Simulations with an idealized GCM. J. Atmos. Sci., 63, 3333–3350, https://doi.org/10.1175/JAS3821.1.
- Wang, Y., P. L. Read, F. Tabataba-Vakili, and R. M. Young, 2018: Comparative terrestrial atmospheric circulation regimes in simplified global circulation models. Part I: From cyclostrophic super-rotation to geostrophic turbulence. *Quart. J. Roy. Meteor. Soc.*, 144, 2537–2557, https://doi.org/10.1002/ qi.3350.
- White, R., D. Battisti, and G. Roe, 2017: Mongolian mountains matter most: Impacts of the latitude and height of Asian orography on Pacific wintertime atmospheric circulation. *J. Climate*, 30, 4065–4082, https://doi.org/10.1175/JCLI-D-16-0401.1.